Journal of the Mechanics and Physics of Solids 64 (2014) 170–183

Contents lists available at ScienceDirect

Journal of the Mechanics and Physics of Solids

journal homepage: www.elsevier.com/locate/jmps

A two-scale model for dynamic damage evolution

Oumar Keita [a], Cristian Dascalu [b,c,*], Bertrand François [a]

[a] Building Architecture and Town Planning Department (BATir) - Université Libre de Bruxelles (ULB), Avenue F.D. Roosevelt, 50 - CPI 194/2 - 1050 Bruxelles, Belgium
[b] UPMC Univ. Paris 06, UMR 7190, Institut Jean-Le-Rond-d'Alembert, 75005 Paris, France
[c] CNRS, UMR 7190, Institut Jean-Le Rond-d'Alembert, 75005 Paris, France

ARTICLE INFO

Article history:
Received 2 May 2013
Received in revised form
26 September 2013
Accepted 6 November 2013
Available online 27 November 2013

Keywords:
Micro-cracks
Dynamic propagation
Homogenization
Damage laws
Wave dispersion

ABSTRACT

This paper presents a new micro-mechanical damage model accounting for inertial effect. The two-scale damage model is fully deduced from small-scale descriptions of dynamic micro-crack propagation under tensile loading (mode I). An appropriate micro-mechanical energy analysis is combined with homogenization based on asymptotic developments in order to obtain the macroscopic evolution law for damage.
Numerical simulations are presented in order to illustrate the ability of the model to describe known behaviors like size effects for the structural response, strain-rate sensitivity, brittle–ductile transition and wave dispersion.

1. Introduction

The failure behavior of quasi-brittle materials is known to be sensitive to internal fractures, at scales of observation smaller than that of the whole structure. For a proper description of this effect a constitutive model involving damage is appropriate. The effect of damage is especially important in phenomena that involve rapid changes of stress level such as earthquakes or underground explosions. At high loading rates, the evolution of damage is sensitive to the rate at which the load is applied. The description of the damage evolution process under dynamic loading of quasi-brittle materials is currently a real scientific challenge. One of the ways to address this issue is the analysis of micro-structural failure process in order to better understand the overall degradation across the material. The modeling of the dynamic damage response requires taking into account the mechanics of micro-cracks and their overall response to applied loading. For this, a model obtained by homogenization from micro-structures with evolving micro-cracks is well suited.

Several models based on micro-mechanics have been developed to study damage process under dynamic compressive response of brittle solids. At the small scale, the damage mechanism usually occurs in mode I (tensile), even if the macroscopic loading is in compression. Nemat-Nasser and Deng (1994) studied an array of interacting and dynamically growing wing cracks and estimated the rate-dependent dynamic damage evolution. Ravichandran and Subhash (1995) developed a micro-mechanical model for ceramics based on non-interacting, uniformly distributed sliding micro-cracks subjected to biaxial dynamic compressive loading and predicted effects of the rate sensitivity on failure strength. Huang et al. (2002) developed a model that combined damage evolution theory with dynamic crack growth under uniaxial dynamic compression. Paliwal and Ramesh (2008) developed a model based on evolution of tensile wing micro-cracks in

* Corresponding author.
E-mail address: cristian.dascalu@upmc.fr (C. Dascalu).

0022-5096/$ - see front matter © 2013 Elsevier Ltd. All rights reserved.
http://dx.doi.org/10.1016/j.jmps.2013.11.003

the case of uniaxial compression under constant strain loading. Bhatt et al. (2011) developed a micro-mechanically motivated damage model for brittle failure at high strain rates and incorporating crack dynamics.

In this paper we propose a new approach for dynamic damage propagation. Considering a locally periodic distribution of evolving micro-cracks, we deduce a dynamic model of damage through the mathematical homogenization method based on asymptotic developments (Benssousan et al., 1978; Sanchez-Palencia, 1980). The obtained model allows for the prediction of advanced features like dependency of the size of the micro-structure, loading rate sensitivity and wave dispersion effects.

A two-scale approach for damage was deduced in Dascalu et al. (2008) for brittle damage. More general formulations of this model, including non-brittle behaviors or more complex crack evolutions, were given in Dascalu (2009), François and Dascalu (2010), Dascalu et al. (2010), Markenscoff and Dascalu (2012). The present development extends these results to the case of dynamic propagation of micro-cracks.

The paper is organized as follows. First, the mathematical formulation of the two-scale problem is presented and the macroscopic damage equations are deduced through the asymptotic homogenization procedure and an energy description of dynamic fracture at the small scale. Then, numerical simulations of the local homogenized response are presented in order to illustrate the ability of the model to reproduce known dynamic behaviors and comparison with experimental data of impact tests is done. Finally, a one-dimensional analysis is performed in order to show that the damage model can predict wave dispersion effects.

2. Two-scale problem

In this paper, we consider the dynamic evolution of the elastic solid containing a large number of micro-cracks (Fig. 1a). We assume that the micro-crack distribution is locally periodic. We denote by ε the size of a periodicity cell or, equivalently, the distance between the centers of neighbor micro-cracks and by l the micro-crack length. The length l is assumed to have small spatial variations such that, locally, the distribution of micro-cracks may be considered as periodic. Each crack is assumed to be parallel to the x_1-axis and straight. We define the damage variable as the ratio between the micro-crack length l and the period size:

$$d = \frac{l}{\varepsilon} \tag{1}$$

taking values between 0 (for undamaged material) and 1 (for completely damaged material).

2.1. Elastodynamics equations

We consider the elastodynamics equations for the initial heterogeneous medium that we assume to be a two-dimensional isotropic elastic medium with micro-cracks. Let $\mathcal{B}_S = \mathcal{B}\backslash\mathcal{C}$ be the solid part of the full domain $\mathcal{B}$, with $\mathcal{C}$ the union of all micro-cracks inside $\mathcal{B}$. The momentum balance equation is

$$\frac{\partial \sigma_{ij}^{\varepsilon}}{\partial x_j} = \rho \frac{\partial^2 u_i^{\varepsilon}}{\partial t^2} \quad \text{in } \mathcal{B}_S \tag{2}$$

and the linear elasticity constitutive relation is

$$\sigma_{ij}^{\varepsilon} = a_{ijkl} e_{xkl}(\mathbf{u}^{\varepsilon}) \tag{3}$$

where a_{ijkl} is the elasticity tensor, $\sigma_{ij}^{\varepsilon}$ is the stress field and u_i^{ε} is the displacement field. The strain tensor is calculated in the small deformations hypothesis:

$$e_{xij}(\mathbf{u}^{\varepsilon}) = \frac{1}{2}\left(\frac{\partial u_i^{\varepsilon}}{\partial x_j} + \frac{\partial u_j^{\varepsilon}}{\partial x_i}\right) \tag{4}$$

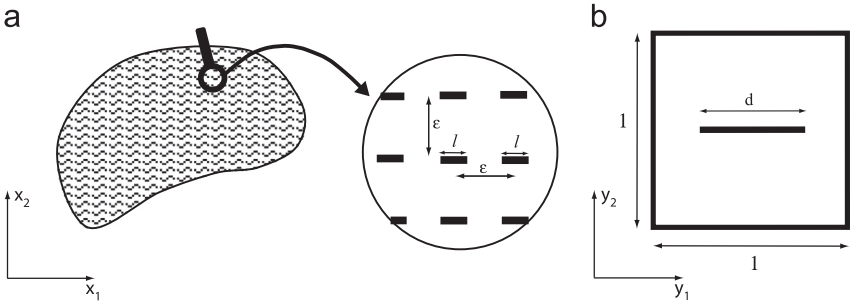

Fig. 1. (a) Micro-fissured medium with locally periodic micro-structure, ε is the size of a period and l is the local micro-crack length. (b) Unit cell with rescaled crack of length d.

where the variables x_i with respect to which the strain tensor is calculated are explicitly mentioned. In the particular case of an isotropic elastic matrix, as considered in the present study, the elasticity tensor is expressed as a function of the elastic constants, the Young Modulus E and the Poisson ratio ν, as follows:

$$a_{ijkl} = \frac{\nu E}{(1+\nu)(1-2\nu)}\delta_{ij}\delta_{kl} + \frac{E}{2(1+\nu)}\left(\delta_{ik}\delta_{jl}+\delta_{il}\delta_{jk}\right) \tag{5}$$

where δ_{ij} is the Kronecker symbol.

Traction free conditions are assumed on the crack faces:

$$\boldsymbol{\sigma}^{\varepsilon}\mathbf{N} = 0 \tag{6}$$

where $\mathbf{N}$ is a unit normal vector on the crack faces (Fig. 2).

2.2. Asymptotic developments

The locally periodic micro-structure is constructed from a reference unit cell Y (Fig. 1b) referred to as microscopic coordinates (y_1,y_2). Rescaled with the small parameter ε, the unit cell becomes the physical period of the material εY as in Fig. 2. The unit cell Y contains the scaled crack CY and we denote by $Y_S = Y|CY$ its solid part.

We assume the micro-structural period ε to be small enough with respect to the characteristic dimensions of the whole body and the wavelength of the elastodynamic fields. In this case, we can distinguish between the microscopic and the macroscopic variations of the mechanical fields. We consider distinct variables at different scales: the macroscopic variable x (at the scale of the whole structure) and the microscopic variable $y = x/\varepsilon$ (at the level of micro-cracks). While the microscopic scale behavior is essentially determined by the presence of the cracks, at the global scale we retrieve a mean (homogeneous) response without seeing the details of micro-heterogeneities. The homogenization procedure allows obtaining this macroscopic behavior by taking into account the micro-structural aspects.

It is also assumed that the macroscopic acceleration is moderate such that the stress gradients are small and no important inertial effects are present at the level of the micro-structural period. In particular, this means that high frequency phenomena like multiple wave reflections on micro-cracks are not explicitly taken into account in the model. In the short wavelength case, when microscopic inertia becomes relevant for the overall behavior, a different upscaling approach should be considered (e.g. Craster et al., 2010).

For a mechanical field depending on both x and y the total spatial derivative takes the form

$$\frac{d}{dx_i} = \frac{\partial}{\partial x_i} + \frac{1}{\varepsilon}\frac{\partial}{\partial y_i} \tag{7}$$

Following the ideas of the asymptotic homogenization method (e.g. Benssousan et al., 1978; Sanchez-Palencia, 1980), we look for two-scale expansions of $\mathbf{u}^{\varepsilon}$ and $\boldsymbol{\sigma}^{\varepsilon}$ in the form:

$$\mathbf{u}^{\varepsilon}(\mathbf{x},t) = \mathbf{u}^{(0)}(\mathbf{x},\mathbf{y},t) + \varepsilon\mathbf{u}^{(1)}(\mathbf{x},\mathbf{y},t) + \varepsilon^2\mathbf{u}^{(2)}(\mathbf{x},\mathbf{y},t) + \cdots \tag{8}$$

$$\boldsymbol{\sigma}^{\varepsilon}(\mathbf{x},t) = \frac{1}{\varepsilon}\boldsymbol{\sigma}^{(-1)}(\mathbf{x},\mathbf{y},t) + \boldsymbol{\sigma}^{(0)}(\mathbf{x},\mathbf{y},t) + \varepsilon\boldsymbol{\sigma}^{(1)}(\mathbf{x},\mathbf{y},t) + \cdots \tag{9}$$

where $\mathbf{u}^{(i)}(\mathbf{x},\mathbf{y},t)$ and $\boldsymbol{\sigma}^{(i)}(\mathbf{x},\mathbf{y},t)$, $\mathbf{x}\in B$, $\mathbf{y}\in Y$ are Y-periodic.

The mass density and the stiffness tensor are assumed to depend on the microscopic variable:

$$\rho^{\varepsilon}(\mathbf{x}) = \rho(\mathbf{y}) = \rho\left(\frac{\mathbf{x}}{\varepsilon}\right) \tag{10}$$

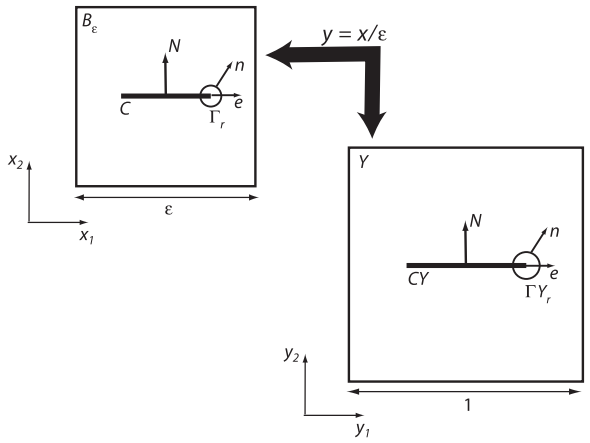

Fig. 2. Rescaling of the unit cell to the microscopic period of the material.

$$a^{\varepsilon}_{ijkl}(\mathbf{x}) = a_{ijkl}(\mathbf{y}) = a_{ijkl}\left(\frac{\mathbf{x}}{\varepsilon}\right) \tag{11}$$

where the functions $\rho(\mathbf{y})$ and $a_{ijkl}(\mathbf{y})$ are Y-periodic.

2.3. Homogenization analysis

Substituting the asymptotic development of $\boldsymbol{\sigma}^{\varepsilon}$ and $\mathbf{u}^{\varepsilon}$ (8) and (9) in the elastodynamic equations (2)–(4) and taking into account the derivation rule (7), one can obtain the following expressions:

$$\frac{\partial \sigma^{(I)}_{ij}}{\partial x_j} + \frac{\partial \sigma^{(I+1)}_{ij}}{\partial y_j} = \rho \frac{\partial^2 u^{(I)}_i}{\partial t^2} \tag{12}$$

$$\sigma^{(I)}_{ij} = a_{ijkl}(e_{xkl}(\mathbf{u}^{(I)}) + e_{ykl}(\mathbf{u}^{(I+1)})) \tag{13}$$

These last equations have to be solved for each I.

(i) Eq. (12) for $I=-2$ and Eq. (13) for $I=-1$ give

$$\frac{\partial \sigma^{(-1)}_{ij}}{\partial y_j} = 0 \tag{14}$$

$$\sigma^{(-1)}_{ij} = a_{ijkl} e_{ykl}(\mathbf{u}^{(0)}) \tag{15}$$

The above equations (14) and (15) lead to boundary value problem of the zero order in ε as follows:

$$\frac{\partial}{\partial y_j}\left(a_{ijkl} e_{ykl}(\mathbf{u}^{(0)})\right) = 0 \quad \text{in } Y_S \tag{16}$$

$$(a_{ijkl} e_{ykl}(\mathbf{u}^{(0)}))N_j = 0 \quad \text{on } CY \tag{17}$$

This shows that the function $\mathbf{u}^{(0)} = \mathbf{u}^{(0)}(\mathbf{x}, t)$ is independent of y variable, representing the macroscopic displacement field.

(ii) Eq. (12) for $I=-1$ and Eq. (13) for $I=0$ give

$$\frac{\partial \sigma^{(0)}_{ij}}{\partial y_j} = 0 \tag{18}$$

$$\sigma^{(0)}_{ij} = a_{ijkl}(e_{xkl}(\mathbf{u}^{(0)} + e_{ykl}(\mathbf{u}^{(1)})) \tag{19}$$

For given $\mathbf{u}^{(0)}$, taking into account Eqs. (18) and (19) one obtains the boundary-value problem for the corrector $\mathbf{u}^{(1)}$:

$$\frac{\partial}{\partial y_j}\left(a_{ijkl} e_{ykl}(\mathbf{u}^{(1)})\right) = 0 \quad \text{in } Y_S \tag{20}$$

$$(a_{ijkl} e_{ykl}(\mathbf{u}^{(1)}))N_j = -(a_{ijkl} e_{xkl}(\mathbf{u}^{(0)}))N_j \quad \text{on } CY \tag{21}$$

with periodicity conditions on the external boundary of the cell. The microscopic corrector $\mathbf{u}^{(1)}$ depends linearly on the macroscopic deformations

$$\mathbf{u}^{(1)}(\mathbf{x}, \mathbf{y}, t) = \boldsymbol{\xi}^{pq}(\mathbf{y}) e_{xpq}(\mathbf{u}^{(0)})(\mathbf{x}, t) \tag{22}$$

Here the characteristic functions $\boldsymbol{\xi}^{pq}(\mathbf{y})$ are elementary solutions of Eqs. (20) and (21) for the particular macroscopic deformations $e_{xij}(\mathbf{u}^{(0)}) = \delta_{ip}\delta_{jq}$ (e.g. Benssousan et al., 1978; Sanchez-Palencia, 1980), where δ_{ip} is the Kronecker symbol. The equilibrium equation (18) shows that inertial effects are not directly present at the microscopic level.

(iii) Eq. (12) for $I=0$ and Eq. (13) for $I=1$ give

$$\frac{\partial \sigma^{(0)}_{ij}}{\partial x_j} + \frac{\partial \sigma^{(1)}_{ij}}{\partial y_j} = \rho \frac{\partial^2 u^{(0)}_i}{\partial t^2} \tag{23}$$

$$\sigma^{(1)}_{ij} = a_{ijkl}(e_{xkl}(\mathbf{u}^{(1)}) + e_{ykl}(\mathbf{u}^{(2)})) \tag{24}$$

By introducing the mean value operator $\langle \cdot \rangle = (1/|Y|)\int_{Y_s} \cdot\, dy$, where $|Y|$ is the area of Y, applying it to Eq. (23) and remembering that $\mathbf{u}^{(0)}$ is y-independent, one can obtain

$$\frac{\partial}{\partial x_j}\langle \sigma^{(0)}_{ij} \rangle = \langle \rho \rangle \frac{\partial^2 u^{(0)}_i}{\partial t^2} \tag{25}$$

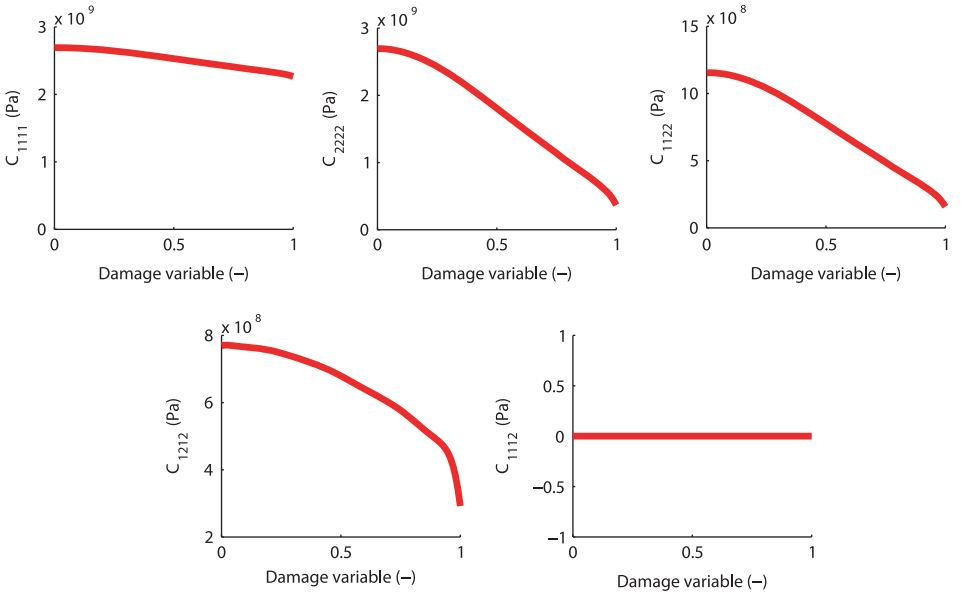

Fig. 3. Homogenized coefficients for elastic parameters $E=2$ GPa and $\nu=0.3$.

We define the macroscopic stress $\Sigma_{ij}^{(0)} \equiv \langle \sigma_{ij}^{(0)} \rangle$ that can be expressed as

$$\Sigma_{ij}^{(0)} = C_{ijkl}(d) e_{xkl}(\mathbf{u}^{(0)}) \tag{26}$$

where

$$C_{ijkl}(d) = \frac{1}{|Y|} \int_{Y_S} \left(a_{ijkl} + a_{ijmn} e_{ymn}\left(\xi^{kl}\right) \right) dy \tag{27}$$

are the homogenized coefficients.

We deduce the dynamic macroscopic behavior:

$$\frac{\partial}{\partial x_j} \Sigma_{ij}^{(0)} = \rho \frac{\partial^2 u_i^{(0)}}{\partial t^2} \tag{28}$$

as describing the overall dynamic behavior of an elastic body with a given distribution of (non-evolving) micro-cracks.

We note that the microscopic stress (19) satisfies the equilibrium equation (18) without inertia effects at the small scale. However, the inertia effects are present at the macroscopic scale, as it can be seen in Eq. (28). This is the result of the separation of scales assumption, leading to relations (12) and (13). Such hypothesis is reasonable for physical phenomena for which the microscopic accelerations have no strong impact on the overall response of the material.

The effective coefficients C_{ijkl} depend on the state of damage and the elastic properties of the solid matrix (E and ν). The coefficients C_{ijkl} defined by (27) can be computed by solving the unit cell problems (20) and (21) for a large number of $d \in [0,1]$. The FEAP finite element code (Taylor, 2008) has been used for the computation of these homogenized coefficients. The obtained effective coefficients are represented in Fig. 3 as functions of the damage variable d.

The presence of the micro-cracks leads to induced anisotropy, the resulting effective elastic response being orthotropic. This is due to predetermined orientations of micro-cracks leading to macroscopic anisotropy even if the solid part of the medium $\mathcal{B}_S$ is assumed to be isotropic (Eq. (5)). We also note the nonlinear dependence of the homogenized coefficients on the damage variable d. With a horizontal crack line (direction 11), the damage-induced loss of rigidity is maximum when the unit cell is loaded in the vertical direction (22), i.e. perpendicular to the crack (coefficients C_{2222} and C_{1122}) while the rigidity is much less affected when loaded in the horizontal direction (11), i.e. parallel to the crack (coefficient C_{1111}). This is characteristic of the damage-induced anisotropy observed at the macro-scale. For $d=1$, the residual value of C_{2222} and C_{1122} is not zero because the micro-crack tips are assumed to remain in contact, even for fully damaged state. It produces a residual rigidity of the unit cell.

3. Energy analysis

In this section we perform a micro-mechanical energy analysis within the homogenization framework. These results will be used in the next section to construct the homogenized dynamic damage laws.

3.1. Dynamic energy release rate

During crack propagation, the dynamic energy release rate can be written as a limit at the tip of a micro-crack as

$$\mathcal{G}^{d\varepsilon} = \lim_{r\to 0}\int_{\Gamma_r} (U+T)n_1 - \sigma_{ij}^{\varepsilon} n_j \frac{\partial u_i^{\varepsilon}}{\partial x_1}\, dS \tag{29}$$

where

$$U = \tfrac{1}{2}\, a_{mnkl} e_{xkl}(\mathbf{u}^{\varepsilon}) e_{xmn}(\mathbf{u}^{\varepsilon}) \tag{30}$$

$$T = \frac{1}{2}\rho \frac{\partial \mathbf{u}^{\varepsilon}}{\partial t}\frac{\partial \mathbf{u}^{\varepsilon}}{\partial t} \tag{31}$$

are respectively the energy of deformation and the kinetic energy densities (Freund, 1998). Here Γ_r is a circle of an infinitesimal radius r surrounding the crack tip and $\mathbf{n}$ is the unit normal vector on Γ_r (see Fig. 2).

We consider a Griffith-type energy criterion: propagation occurs when a critical energy threshold $\mathcal{G}_c$ is reached. The crack propagation is described by the following relations:

$$\mathcal{G}^{d\varepsilon} \le \mathcal{G}_c; \quad \frac{dl}{dt} \ge 0; \quad \frac{dl}{dt}\left(\mathcal{G}^{d\varepsilon} - \mathcal{G}_c\right) = 0 \tag{32}$$

where $\mathcal{G}_c$ is the critical fracture energy of the material.

Similar to the quasi-static case (Dascalu et al., 2008), one can establish the scaling relation:

$$\mathcal{G}^{d\varepsilon} = \varepsilon \mathcal{G}_y^d \tag{33}$$

with

$$\mathcal{G}_y^d = \lim_{r\to 0}\int_{\Gamma Y_r} -a_{ijkl}\left(e_{ykl}(\mathbf{u}^{(1)}) n_j \left(\frac{\partial u_i^{(1)}}{\partial y_1}\right)\right) + \left(\frac{1}{2} a_{mnkl} e_{ykl}(\mathbf{u}^{(1)}) e_{ymn}(\mathbf{u}^{(1)}) + \frac{1}{2}\rho c^2 \left(\frac{\partial \mathbf{u}^{(1)}}{\partial y_1}\right)^2\right) n_1\, ds_y \tag{34}$$

In order to prove the above relation, we start with the first order terms in the development of strain and stress as results from (8) and (9):

$$e_{xkl}(\mathbf{u}^{\varepsilon}) = e_{xkl}(\mathbf{u}^{(0)}) + e_{ykl}(\mathbf{u}^{(1)}) \tag{35}$$

$$\sigma_{ij}^{\varepsilon} = a_{ijkl}(e_{xkl}(\mathbf{u}^{(0)}) + e_{ykl}(\mathbf{u}^{(1)})) \tag{36}$$

Substituting these expressions in Eqs. (30) and (31), we get

$$U = \tfrac{1}{2}\, a_{mnkl}\left(e_{xkl}(\mathbf{u}^{(0)}) + e_{ykl}(\mathbf{u}^{(1)})\right)\left(e_{xmn}(\mathbf{u}^{(0)}) + e_{ymn}(\mathbf{u}^{(1)})\right) \tag{37}$$

$$T = \frac{1}{2}\rho c^2 \left(\frac{\partial(\mathbf{u}^{(0)} + \varepsilon \mathbf{u}^{(1)})}{\partial x_1}\right)^2 \tag{38}$$

Eq. (38) is obtained according to the behavior of the displacement near the moving crack tip for r close to 0 (Freund, 1998):

$$\frac{\partial \mathbf{u}^{\varepsilon}}{\partial t} = -c\frac{\partial \mathbf{u}^{\varepsilon}}{\partial x_1} \tag{39}$$

where c is the speed of crack propagation.

Substitution of $\sigma_{ij}^{\varepsilon}$, $\mathbf{u}^{\varepsilon}$, T and U in Eq. (29) gives

$$\mathcal{G}^{d\varepsilon} = \lim_{r\to 0}\int_{\Gamma Y_r} \left(-a_{ijkl}\left(e_{xkl}(\mathbf{u}^{(0)}) + e_{ykl}(\mathbf{u}^{(1)})\right) n_j \left(\frac{\partial u_i^{(0)}}{\partial x_1} + \frac{\partial u_i^{(1)}}{\partial y_1}\right) + \left(\frac{1}{2} a_{mnkl}\left(e_{xkl}(\mathbf{u}^{(0)}) + e_{ykl}(\mathbf{u}^{(1)})\right)\left(e_{xmn}(\mathbf{u}^{(0)}) + e_{ymn}(\mathbf{u}^{(1)})\right)\right.$$
$$\left. + \frac{1}{2}\rho c^2 \left(\frac{\partial \mathbf{u}^{(0)}}{\partial x_1} + \frac{\partial \mathbf{u}^{(1)}}{\partial y_1}\right)^2\right) n_1\right) \varepsilon\, ds_y \tag{40}$$

where the change of variables $dS = \varepsilon ds_y$ has been done in the integral (40). By taking into account the singularity of $\mathbf{u}^{(1)}$ at the crack tip (Freund, 1998) we can obtain the following relation:

$$\mathcal{G}^{d\varepsilon} = \varepsilon \lim_{r\to 0}\int_{\Gamma Y_r} -a_{ijkl}\left(e_{ykl}(\mathbf{u}^{(1)}) n_j \left(\frac{\partial u_i^{(1)}}{\partial y_1}\right)\right) + \left(\frac{1}{2} a_{mnkl} e_{ykl}(\mathbf{u}^{(1)}) e_{ymn}(\mathbf{u}^{(1)}) + \frac{1}{2}\rho c^2 \left(\frac{\partial \mathbf{u}^{(1)}}{\partial y_1}\right)^2\right) n_1\, ds_y \tag{41}$$

where in the right member we recognize the scaled energy-release rate $\mathcal{G}_y^d$. This proves the relation (33).

As we showed in the previous section, the cell problem (20) and (21) obtained in dynamics is identical with the one obtained in quasi-statics (Dascalu et al., 2008).

The scaled energy release rate (34) can be decomposed as

$$\mathcal{G}_y^d = \lim_{r\to 0}\int_{\Gamma Y_r} -a_{ijkl}\left(e_{ykl}(\mathbf{u}^{(1)})n_j\left(\frac{\partial u_i^{(1)}}{\partial y_1}\right)\right) + \left(\frac{1}{2}a_{mnkl}e_{ykl}(\mathbf{u}^{(1)})e_{ymn}(\mathbf{u}^{(1)})\right)n_1\, ds_y + \lim_{r\to 0}\int_{\Gamma Y_r} + \frac{1}{2}\rho c^2\left(\frac{\partial \mathbf{u}^{(1)}}{\partial y_1}\right)^2 n_1\, ds_y \tag{42}$$

The first integral of the right member of Eq. (42) is denoted by $\mathcal{G}_y$ and represents the scaled quasi-static energy release rate (Dascalu et al., 2008), here calculated with the dynamic corrector.

Thus the relation between dynamic and quasi-static scaled energy release rates can be written as

$$\mathcal{G}_y^d = \mathcal{G}_y + \frac{1}{2}\rho c^2 \lim_{r\to 0}\int_{\Gamma Y_r}\left(\frac{\partial \mathbf{u}^{(1)}}{\partial y_1}\right)^2 n_1\, ds_y \tag{43}$$

and by using (33) we obtain

$$\mathcal{G}^{d\varepsilon} = \mathcal{G}^{\varepsilon} + \varepsilon\frac{1}{2}\rho c^2 \lim_{r\to 0}\int_{\Gamma Y_r}\left(\frac{\partial \mathbf{u}^{(1)}}{\partial y_1}\right)^2 n_1\, ds_y \tag{44}$$

where $\mathcal{G}^{\varepsilon} = \varepsilon\mathcal{G}_y$.

3.2. Dynamic energy release rate and stress intensity factors

For an isotropic elastic medium, as assumed in the present study (Eq. (5)), the physical energy release rate in dynamics is expressed as a function of the stress intensity factors as follows (Freund, 1998):

$$\mathcal{G}^{d\varepsilon} = \frac{1-\nu^2}{E}A(\dot{l})(K_I^{d\varepsilon})^2 \tag{45}$$

where $K_I^{d\varepsilon}$ represents the dynamic stress intensity factor and $A(\dot{l})$ is a universal function of the crack speed. For the tensile crack growth at nonuniform speed, $K_I^{d\varepsilon}$ can be expressed following Freund (1998) as

$$K_I^{d\varepsilon} = k(\dot{l})K_I^{\varepsilon} \tag{46}$$

where K_I^{ε} is the static stress intensity factor that would have resulted from the applied loading if the crack tip had always been at its instantaneous position represented by $l(t)$.

By substituting Eq. (46) into Eq. (45) we can obtain the following relation:

$$\mathcal{G}^{d\varepsilon} = \frac{1-\nu^2}{E}A(\dot{l})k^2(\dot{l})(K_I^{\varepsilon})^2 \tag{47}$$

For crack propagation in mode I, Freund (1998) established the relation

$$A(\dot{l})k^2(\dot{l}) = \left(1-\frac{\dot{l}}{C_R}\right) \tag{48}$$

where C_R is Rayleigh wave speed and can be expressed by

$$C_R = \frac{0.862+1.14\nu}{1+\nu}\sqrt{\frac{E}{2\rho(1+\nu)}} \tag{49}$$

By replacing (48) into (47), the physical energy release rate on dynamic load conditions becomes

$$\mathcal{G}^{d\varepsilon} = \frac{1-\nu^2}{E}(K_I^{\varepsilon})^2 - \frac{\dot{l}}{C_R}\frac{1-\nu^2}{E}(K_I^{\varepsilon})^2 \tag{50}$$

Comparing Eq. (44) to Eq. (50) the following equality can be identified:

$$\varepsilon\frac{1}{2}\rho c^2 \lim_{r\to 0}\int_{\Gamma_r}\left(\frac{\partial \mathbf{u}^{(1)}}{\partial y_1}\right)^2 n_1\, ds_y = -\frac{\dot{l}}{C_R}\frac{1-\nu^2}{E}(K_I^{\varepsilon})^2 \tag{51}$$

4. Dynamic damage evolution

The effective constitutive law presented in Section 2 (Eq. (26)) enables us to compute the stress–strain behavior of the material at a given state of non-evolving damage. In this section, by assuming that the micro-cracks evolve, we deduce the corresponding macroscopic damage evolution.

Under a given loading of the macroscopic structure, the resulting local state of stress leads to the activation of particular families of micro-cracks. In what follows, we place ourselves in such a macroscopic point and we assume that in a small vicinity a family of straight micro-cracks is activated and they are propagating in mode I, symmetrically with respect to their middle-point.

To deduce the macroscopic damage equation we will follow the method developed in Dascalu et al. (2008) for brittle micro-fracture and Dascalu (2009) for quasi-brittle or subcritical micro-crack evolutions. In these contributions a general damage model has been obtained by homogenization in the quasi-static framework. These results are extended here to the case of dynamic propagation of micro-cracks including inertial effects in the momentum balance. Although we will consider a brittle-type propagation criterion at the micro-scale, we will show that including the inertial effects may lead to non-brittle overall responses.

In Dascalu et al. (2008) the following relation was deduced, based on quasi-static evolution of micro-cracks:

$$\frac{dd}{dt}\left(\frac{1}{2}\frac{\partial C_{ijkl}(d)}{\partial d}e_{xkl}(\mathbf{u}^{(0)})e_{xij}(\mathbf{u}^{(0)})+\mathcal{G}_y\right)=0 \tag{52}$$

This relation still holds in our case if $\mathcal{G}_y$ represents the scaled quasi-static energy release rate calculated with the dynamic corrector as explained in Section 3.

By replacing (44) in (52) with $\mathcal{G}^{\varepsilon}=\varepsilon\mathcal{G}_y$ and considering (33) we obtain

$$\frac{dd}{dt}\left(\frac{1}{2}\frac{\partial C_{ijkl}(d)}{\partial d}e_{xkl}(\mathbf{u}^{(0)})e_{xij}(\mathbf{u}^{(0)})+\frac{\mathcal{G}^{d\varepsilon}}{\varepsilon}-\frac{1}{2}\rho c^2\lim_{r\to 0}\int_{\Gamma_r}\left(\frac{\partial \mathbf{u}^{(1)}}{\partial y_1}\right)^2 n_1\, ds_y\right)=0 \tag{53}$$

Considering the relation (51), we obtain

$$\frac{dd}{dt}\left(\frac{1}{2}\frac{\partial C_{ijkl}(d)}{\partial d}e_{xkl}(\mathbf{u}^{(0)})e_{xij}(\mathbf{u}^{(0)})+\frac{\mathcal{G}^{d\varepsilon}}{\varepsilon}+\frac{\varepsilon\dot{d}}{C_R}\frac{1-\nu^2}{E\varepsilon}(K_I^{\varepsilon})^2\right)=0 \tag{54}$$

By replacing $(K_I^{\varepsilon})^2$ by its expression as a function of $\mathcal{G}^{d\varepsilon}$, as deduced from (50), it leads to the dynamic damage equation as follows:

$$\frac{dd}{dt}\left(\frac{1}{2}\frac{\partial C_{ijkl}(d)}{\partial d}e_{xkl}(\mathbf{u}^{(0)})e_{xij}(\mathbf{u}^{(0)})+\frac{\mathcal{G}^{d\varepsilon}}{\varepsilon}\left(1+\frac{\varepsilon\dot{d}}{C_R-\varepsilon\dot{d}}\right)\right)=0 \tag{55}$$

Finally, when the Griffith criterion (32) is satisfied, we have $\mathcal{G}^{d\varepsilon}=\mathcal{G}_c$ and we obtain the dynamic damage equation as follows:

$$\frac{dd}{dt}\left(\frac{1}{2}\frac{\partial C_{ijkl}(d)}{\partial d}e_{xkl}(\mathbf{u}^{(0)})e_{xij}(\mathbf{u}^{(0)})+\frac{\mathcal{G}_c}{\varepsilon}\left(1+\frac{\varepsilon\dot{d}}{C_R-\varepsilon\dot{d}}\right)\right)=0 \tag{56}$$

The other two relations corresponding to (32) can be obtained in a similar way.

Upon micro-crack propagation, we can see that the quasi-static damage equation (52) represents the limit case of the dynamic damage equation (56) when $\dot{l}/C_R \ll 1$. This means that when the crack propagation speed $\dot{l}$ is very small compared to the material Rayleigh wave speed C_R, the dynamic damage equation corresponds to the quasi-static case.

One of the fundamental assumptions of the mathematical homogenization theory (Benssousan et al., 1978; Sanchez-Palencia, 1980) is that the size of the heterogeneity is infinitely small. This means that, once the asymptotic developments have been inserted in the field equations, the macroscopic equations are obtained by considering the limit $\varepsilon\to 0$. In this limit, by considering vanishingly small micro-structural periods, we actually neglect the aspects related to the finite size of the micro-structure.

For models not depending on the micro-structural size, like the linear elasticity theory, this limit does not change the initial form of the equations. This is the case for general size-independent models. But this is not true for the damage evolution equation (56) in which ε explicitly appears. The damage equation (56) inherits the features of the micro-fracture laws (32) that represent a size-dependent model.

In the present contribution we adopt the point of view of the asymptotic analysis, by studying the macroscopic system represented by Eqs. (26), (28) and (56) for small values of the micro-structural parameter ε. This type of approach has been considered, for instance, in Smyshlyaev and Cherednichenko (2000), Peerlings and Fleck (2004), Tran et al. (2012) in order to obtain strain gradient elasticity models.

Finally, for evolving damage, we can rewrite (56) in the form:

$$\frac{dd}{dt}=\frac{2C_R}{\varepsilon}\left(\frac{\mathcal{G}_c}{\varepsilon\dfrac{\partial C_{ijkl}(d)}{\partial d}e_{xkl}(\mathbf{u}^{(0)})e_{xij}(\mathbf{u}^{(0)})}+\frac{1}{2}\right) \tag{57}$$

as the dynamic evolution law for damage.

5. Local macroscopic response

For the analysis of the homogenized response in a macroscopic point, the input of Eq. (57) is the macroscopic strain $e_{xkl}(u^{(0)})$ at each time t.

For the given macroscopic strain history $e_{xkl}(u^{(0)})$, the damage evolution equation (57) is solved by using an explicit time integration scheme. The corresponding homogenized coefficients $C_{ijkl}(d)$ and the macroscopic stress $\Sigma_{ij}^{(0)} = C_{ijkl}(d)e_{xkl}(u^{(0)})$ are then computed.

We perform tension tests at constant strain rate, with the only non-vanishing component $\dot{e}_{22}$. The numerical values of the parameters used in the simulations are given in Table 1. They represent the reference parameters of the numerical simulations performed below. However, in order to study the influence of the key parameters of the model, the following sub-sections consider varying values of ε, $\dot{e}_{22}$ and d_0.

5.1. Influence of micro-structure size ε

At constant $\mathcal{G}_c$, C_R and imposed strain rate $\dot{e}_{22}$ (numerical values reported in Table 1), the decrease of the micro-structure size ε produces an increase of the tensile strength together with an important reduction of ductility (Fig. 4). On the one hand, the strength increase is explained by the activation of damage propagation criterion which depends on the micro-structure size ε. Smaller micro-structures are more resistant to damage. This known effect has been retrieved also in the quasi-static models of damage (Dascalu et al., 2008; Dascalu, 2009) obtained by a similar homogenization procedure. As remarked before, the quasi-static model is obtained from Eq. (56) for crack propagation speed much smaller than the Rayleigh wave speed. On the other hand, the decrease of the micro-structural size leads to a more brittle macroscopic response. This effect is specific to dynamics since it is not present in the quasi-static two-scale approaches obtained previously.

The effect of micro-structure size on the peak stress is mainly marked for small size. On the contrary, as shown in Fig. 5, for larger micro-structure size this strength tends asymptotically to a constant value which is no more affected by ε.

The strengthening of the material with decreasing micro-structural size is the consequence of the damage law (in which the size ε appears) deduced from the Griffith fracture criterion assumed at the micro-scale. Except the periodicity hypothesis, no micro-crack interactions are considered. In this case, each crack has an independent evolution and, following the energy criterion, larger cracks propagate easier than smaller ones. This explains the dependency on ε predicted by the model. It expresses the Linear Elastic Fracture Mechanics size effect (Bazant, 2002) upscaled to damage at the macro-level.

We finally remark that the present analysis assumes a critical fracture energy $\mathcal{G}_c$ independent on the micro-structural size ε. A different approach may be obtained by considering in the damage law (57) a function $\mathcal{G}_c(\varepsilon)$ determined experimentally, in order to predict more specific size effects.

5.2. Influence of the rate of loading

The macroscopic responses for different rates of loading are represented in Fig. 6, for $\varepsilon = 10^{-3}$ m. We remark that the rate of loading does not affect the initiation of damage. However, it affects the ductility of the macroscopic response. While for low strain rates the stress and damage evolution are brittle, for higher strain rates the response is much more ductile.

The obtained strain rate influence can be explained by the competition between the deformation of the elastic matrix and the evolution of micro-cracks. For low strain rates the damage evolution is dominant leading to brittle response, while for high strain rates the damage evolution is slower than the loading rate, leading to a more ductile response.

In this way, the increase of the strain rate leads to a transition from brittle to ductile behavior.

Table 1
Numerical values of parameters used in the simulations.

E (Pa)	ν (–)	ε (m)	$\dot{e}_{11}$ (s^{-1})	$\dot{e}_{22}$ (s^{-1})	$\mathcal{G}_c$ (J/m^2)	ρ (kg/m^3)	d_0 ($\cdot$)
3×10^{11}	0.22	10^{-3}	0	1×10^3	50.752	3800	0.2

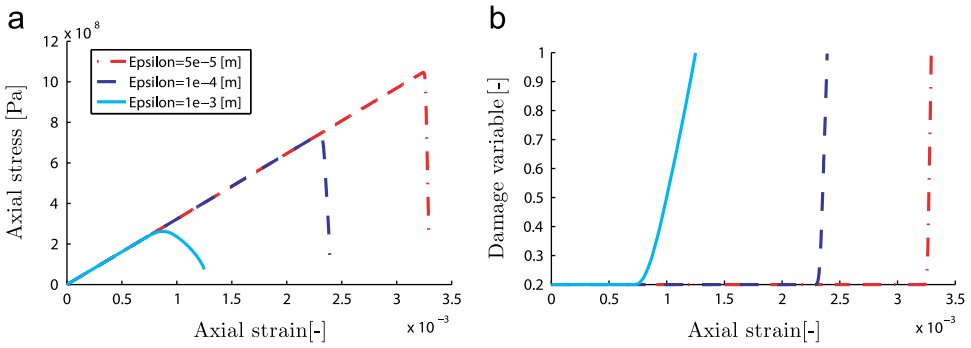

Fig. 4. Effect of the internal length ε for a tension test at constant strain rate. Evolution of (a) stress (b) damage variable with strain.

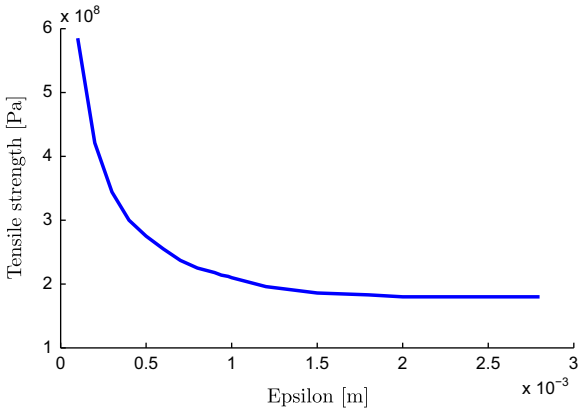

Fig. 5. Evolution of the peak stress as a function of the micro-structural size ε, for a tension test at constant strain rate.

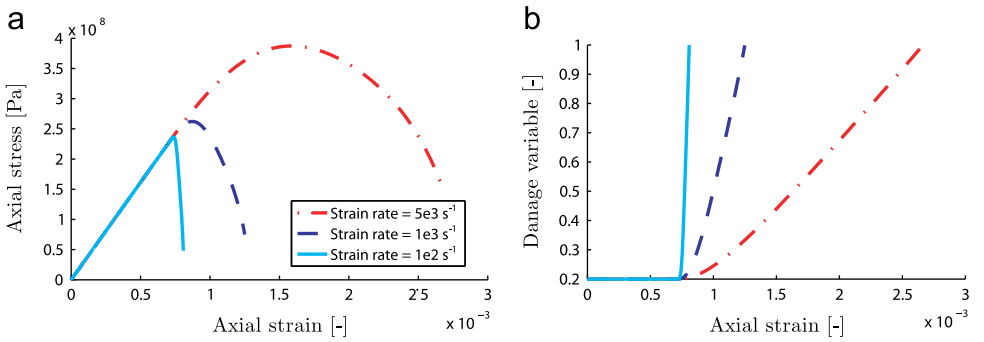

Fig. 6. Effect of the strain rate $\dot{e}_{22}$ on the macroscopic response, for $\varepsilon = 10^{-3}$ m. Evolution of (a) stress and (b) damage variable with strain.

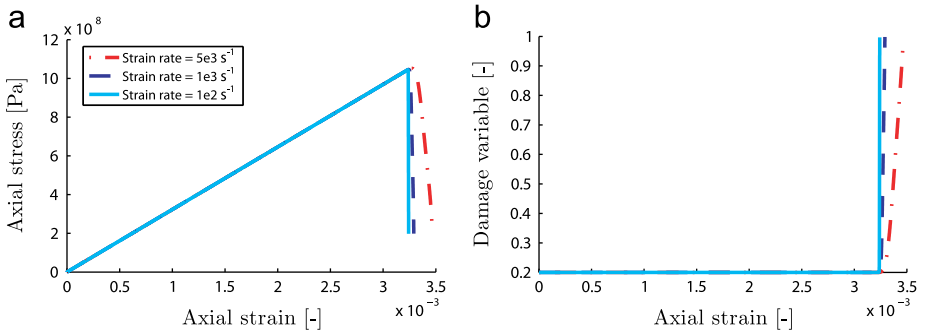

Fig. 7. Effect of the strain rate $\dot{e}_{22}$ on the macroscopic response, for $\varepsilon = 5 \times 10^{-5}$ m. Evolution of (a) stress and (b) damage variable with strain.

In Fig. 7 we represented the responses for different strain rates when $\varepsilon = 5 \times 10^{-5}$ m. We remark that the effect of small values of ε, leading to very brittle behavior, is dominant. The strength and ductility increase with the strain rate become negligible for such values of the micro-structural length.

5.3. *Influence of the initial damage*

The macroscopic responses for different initial damage values are represented in Fig. 8. As expected, the strength and the stiffness increase with the decreasing initial damage d_0. The damage evolution is governed by the damage law (56). It predicts initiation of damage evolution from d_0 for a particular value of the macroscopic deformation. The initial stiffness depends on the initial damage through the homogenized coefficients, this stiffness being lower when the initial damage is higher. For higher initial values of d_0, the damage evolves more rapidly leading to lower strength values.

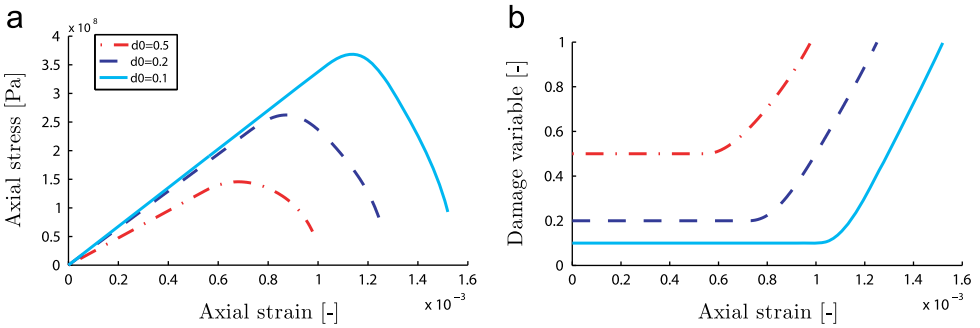

Fig. 8. Effect of initial damage d_0 on the macroscopic response. Evolution of (a) stress and (b) damage variable with strain.

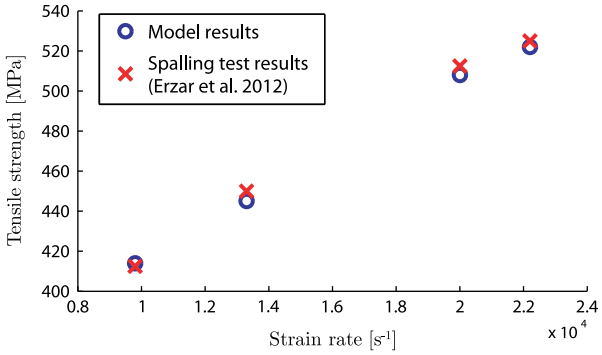

Fig. 9. Strain-rate sensitivity of tensile strength: comparison of model results with spalling test results.

6. Model validation

In order to validate our dynamic damage model, we use the results of spalling tests carried out by Erzar and Buzaud (2012) on AL23 alumina ceramic through the isentropic pressure wave generator machine (GEPI). The GEPI test generates a uniaxial compressive wave in the specimen and the fragmentation occurs in a state of uniaxial strain. The dynamic tensile strength of the tested alumina ceramic is directly computed by the classical acoustic approximation formulated by Novikov et al. (1966):

$$\sigma_{spalling} = \tfrac{1}{2}\,\rho C_L \Delta V_{pb} \tag{58}$$

In this equation, the ultimate tensile stress $\sigma_{spalling}$ is directly linked to the density ρ, the wave speed C_L and the pullback velocity ΔV_{pb}. This last term corresponds to the difference between the maximum velocity measured on the rear free-surface and the first rebound of velocity which is the evidence of the tensile damage within the core of the tested sample.

To prove our model efficiency we compare the strain-rate sensitivity of tensile strength curve of AL23 alumina ceramic from the GEPI tests (Erzar and Buzaud, 2012) with the results obtained after calibration of our model (Fig. 9). The physical parameters of the AL23 alumina ceramic have been considered ($E=300$ GPa; $\nu=0.3$; $\mathcal{G}_c = 50.752$ J/m^2; $\rho=3800$ kg/m^3). The corresponding homogenized coefficients have been computed as a function of damage state with the FEAP finite element code.

For the micro-structural size of $\varepsilon = 3 \times 10^{-4}$ and initial damage values $d_0 = 0.3$, the dynamic damage model gives a good agreement with the experimental results, as can be seen in Fig. 9.

Due to the lack of experimental data on the micro-structural characteristics of the material, the determination of d_0 and ε has been done by calibration in order to get the best agreement with the experimental results. So, it is worth mentioning that the results of Fig. 9 consist mainly in calibration rather than blind predictions, even if E, ν, ρ and $\mathcal{G}_c$ have been taken as close as possible to the representative values of AL23 alumina ceramic.

7. Wave dispersion analysis

Wave propagation in micro-structured materials is strongly affected by processes at internal space scales and many attempts have been made to model these effects (Kunin, 1983; Capriz, 1989; Erofeeyev, 2003). They are particularly important for micro-fractured solids, in which wave dispersion phenomena are observed. In this section we perform a one-dimensional dispersion analysis for the dynamic damage model developed in Section 4.

In the 1D framework, the equation of elastodynamics becomes

$$\frac{\partial}{\partial x}\left(C_{2222}(d)e_{x22}(u^{(0)})\right)=\langle\rho\rangle\frac{\partial^2 u_2^{(0)}}{\partial t^2} \tag{59}$$

Since we aim obtaining analytical results, we approximate the homogenized coefficient $C_{2222}(d)$ by the formula

$$C_{2222}(d)=\tfrac{1}{3}(3-d^2-2d)E \tag{60}$$

Substituting (60) into (59) we get

$$-\tfrac{2}{3}(1-d)Ed'e_{x22}+\tfrac{1}{3}(3-d^2-2d)Ee'_{x22}=\langle\rho\rangle\ddot{u}_2^{(0)} \tag{61}$$

where we used the notation $e'=\partial e/\partial x$.

The dynamic damage evolution law (57) can be rewritten in the form

$$\dot{d}(1-d)e_{x22}^2=A_1+A_2(1-d)e_{x22}^2 \tag{62}$$

with $A_1=3C_R\mathcal{G}_c/-\varepsilon^2E$ and $A_2=C_R/\varepsilon$.

To illustrate the presence of dispersion we consider the linearization of Eqs. (61) and (62) around a constant state of strain and damage variables (ξ,D):

$$e_{x22}=\xi+\xi_0(x,t) \tag{63}$$

$$d=D+d_0(x,t) \tag{64}$$

Substitution of (63) and (64) into (61) and (62) gives the linearized expressions of the damage evolution law (62) and the elastodynamics equation (61) as

$$(1+D)\xi^2\dot{d}_0=A_1+A_2(1+D)\xi^2+2A_2(1+D)\xi\xi_0+A_2\xi^2d_0 \tag{65}$$

$$-\frac{2}{3}(1+D)E\xi d_0'+\frac{1}{3}(3-D^2-2D)E\xi_0'=\langle\rho\rangle\ddot{u}_2^{(0)} \tag{66}$$

Introducing the change of variable

$$d_0^*=d_0+\frac{A_1+A_2(1+D)\xi^2}{A_2\xi^2} \tag{67}$$

Eqs. (65) and (66) become

$$(1+D)\xi^2\dot{d}_0^*=2A_2(1+D)\xi\xi_0+A_2\xi^2d_0^* \tag{68}$$

$$-\tfrac{2}{3}(1+D)E\xi d_0^{*'}+\tfrac{1}{3}(3-D^2-2D)E\xi_0'=\langle\rho\rangle\ddot{u}_2^{(0)} \tag{69}$$

respectively.

From (63) we get for the displacement variable $u_2^{(0)}=\xi x+u_{02}^{(0)}(x,t)$ and (69) can be rewritten as

$$-\tfrac{2}{3}(1+D)E\xi d_0^{*'}+\tfrac{1}{3}(3-D^2-2D)Eu_{02}^{(0)''}=\langle\rho\rangle\ddot{u}_{02}^{(0)} \tag{70}$$

Consider a harmonic excitation for the displacement and damage variables:

$$u_{02}^{(0)}(x,t)=u_1e^{i(kx-\omega t)},\quad d_0^*(x,t)=d_1e^{i(kx-\omega t)} \tag{71}$$

where i is the imaginary unit, ω is the circular frequency and k is the wave number. We remark that the present analysis should be applied only to the regime of increasing values of the damage variable.

By substituting (71) into (68) and (70) we get the set of equations

$$-(1+D)i\xi^2\omega d_1-2A_2(1+D)ik\xi u_1-A_2\xi^2d_1=0 \tag{72}$$

$$-\tfrac{2}{3}(1+D)i\xi kd_1-\tfrac{1}{3}(3-D^2-2D)Ek^2u_1+\langle\rho\rangle\omega^2u_1=0 \tag{73}$$

A non-trivial solution exists for the system formed by (72) and (73) if

$$\det\begin{pmatrix}(A_2\xi^2-(1+D)i\xi^2\omega) & (-2A_2(1+D)ik\xi)\\ \left(-\tfrac{2}{3}(1+D)Ei\xi k\right) & \left(\langle\rho\rangle\omega^2-\tfrac{1}{3}(3-D^2-2D)Ek^2\right)\end{pmatrix}=0 \tag{74}$$

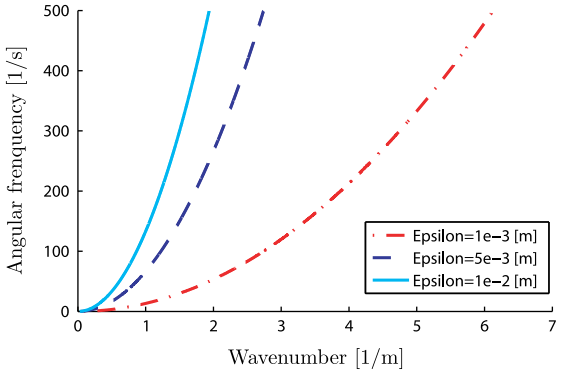

Fig. 10. Dispersion curves for different values of the internal length ε.

This allows us to determine dispersion equation as

$$-\omega^2-\frac{(1+D)i\omega^3\varepsilon}{C_R}+\frac{(7+3D^2+6D)Ek^2}{3\langle\rho\rangle}+\frac{(1+D)(3-D^2-2D)ik^2E\varepsilon\omega}{3C_R\langle\rho\rangle}=0 \tag{75}$$

where the expression of A_2 in (62) has been taken into account.

Let us denote $B_1=(1+D)\omega^3\varepsilon/C_R$, $B_2=(7+3D^2+6D)Ek^2/3\langle\rho\rangle$ and $B_3=(1+D)(3-D^2-2D)E\varepsilon\omega/3C_R\langle\rho\rangle$. If we consider the wave number to be complex $k=k_1+ik_2$, then k_1 characterizes the propagation ($v_{ph}=\omega/k_1$ is phase velocity of the wave), and k_2 characterizes wave dissipation. Eq. (75) can be solved analytically and for k_1 we obtain

$$k_1=\pm\sqrt{\frac{B_1B_3+\omega^2B_2}{2(B_2^2+B_3^2)}\pm\sqrt{\frac{1}{4}\left(\frac{B_1B_3+\omega^2B_2}{(B_2^2+B_3^2)}\right)^2+\left(\frac{-\omega^2}{2B_3}+\frac{-\omega^2+B_1B_2B_3+\omega^2B_2}{2(B_2^2+B_3^2)B_3}\right)^2}} \tag{76}$$

Taking the positive value of k_1, which corresponds to the $+$ sign, we represented in Fig. 10 the dispersion curves for different values of the internal length ε. The curves depend essentially on the micro-structural length which controls the dispersion effects.

The dispersion effects appear as a consequence of the presence of the micro-structural parameter ε in the damage law (56). This law predicts that the dispersion effects are not present if the damage does not evolve. They are intimately related with damage evolution: the waves interact with micro-cracks making them propagate and this change of micro-structure affects the wave properties. The size parameter ε, representing the distance between centers of neighbor micro-cracks, influences this evolution. We note that wave dispersion effects due to inelastic dissipation have been already considered by different authors (Liu et al., 1976; Müller et al., 2010). In our case, the inelastic behavior is that given by the evolution of damage.

In Section 5.1 we showed that the damage evolution is more rapid for bigger values of ε. This results in a more important amount of energy dissipated for micro-crack propagation. Since the dispersion effects are directly related to the way in which damage evolves it is expected that they amplify with the increase of the micro-structural size ε. This is what the model predicts as it can be observed in Fig. 10.

We finally note that such effects of the internal length on wave dispersion are also retrieved in the nonlocal models (e.g. Papargyri-Beskou et al., 2009 for gradient elasticity), even if the physical origin is different.

8. Conclusions

A new damage model that accounts for dynamic effects has been proposed. The damage evolution law has been completely deduced by asymptotic homogenization coupled with microscopic energy analysis for a locally periodic distribution of micro-cracks propagation which propagate dynamically.

For real finite-sized micro-structures, the dynamic damage law contains a micro-structural length allowing for the prediction of size effects. It has been shown that the presence of the micro-structural length also controls the wave dispersion effects.

For low rate of loading, the damage model tends to the quasi-static criterion with a brittle response while the high rate of loading produces a ductile behavior governed by inertial effect. The model incorporates strain-rate sensitivity of tensile strength and the stress–strain behavior. Validation of the model is performed by comparing strain-rate dependency of the tensile strength with the corresponding experimental results obtained from the spalling test.

In the present model, we assumed a locally periodic distribution of micro-cracks, with smooth variations of the crack length at the macro-scale. One may combine the energy analysis for dynamic crack propagation at the micro-scale with other upscaling schemes, like the ones assuming homogeneous strain or stress on the boundary of the elementary volume or for non-periodic micro-structures (Briane, 1994).

The present approach may be extended to compression loadings by considering wing-type cracks or crack emanating from pores. Under compression loadings, such cracks are extending in mode I and one may construct a specific damage model by homogenization by following the same lines as in the present approach.

Acknowledgments

The research of C. Dascalu was funded by the Grant GEOBRIDGE ANR-09- BLAN-0096-01 of the French National Agency for Research. O. Keita acknowledges the Islamic Development Bank (IDB) scholarship program for the financial support of this work.

References

Bazant, Z.P., 2002. Scaling of Structural Strength. Hermes Penton Science, London.
Bhatt, H., Rosakis, A., Sammis, G., 2011. A micro-mechanics based constitutive model for brittle failure at high strain rates. J. Appl. Mech. 79 (3), 1016–1028.
Benssousan, A., Lions, J., Papanicolaou, G., 1978. Asymptotic Analysis for Periodic Structures. Kluwer Academic Publisher, Amsterdam.
Briane, M., 1994. Homogenization of a nonperiodic material. J. Math. Pure Appl. (9) 73 (1), 47–66.
Capriz, G., 1989. Continua with Microstructure. Springer, Heidelberg.
Craster, R.V., Kaplunov, J., Pichugin, A.V., 2010. High frequency homogenization for periodic media. Proc. R. Soc. A 466, 2341–2362.
Dascalu, C., François, B., Keita, O., 2010. A two-scale model for subcritical damage propagation. Int. J. Solids Struct. 47, 493–502.
Dascalu, C., Bilbie, G., Agiasofitou, E., 2008. Damage and size effect in elastic solids: a homogenization approach. Int. J. Solid Struct. 45, 409–430.
Dascalu, C., 2009. A two-scale damage model with material length. C. R. Mec. 337, 645–652.
Erzar, B., Buzaud, E., 2012. Shockless spalling damage of alumina ceramic. Eur. Phys. J. Spec. Top. 206, 71–77.
Erofeeyev, V.I., 2003. Wave Processes in Solids with Microstructure. World Scientific, Singapore.
François, B., Dascalu, C., 2010. A two-scale time-dependent damage model based on non-planar growth of micro-cracks. J. Mech. Phys. Solids 58, 1928–1946.
Freund, L.B., 1998. Dynamic Fracture Mechanics. Cambridge University Press.
Huang, C., Subhash, G., Vitton, S.J., 2002. A dynamic damage growth model for uniaxial compressive response of rock aggregates. Mech. Mater. 34, 267–277.
Kunin, I.A., 1983. Elastic Media with Microstructure II. Three-Dimensional Models. Springer, Berlin.
Liu, H.P., Anderson, D.L., Kanamori, H., 1976. Velocity dispersion due to anelasticity; implication for seismology and mantle composition. Geophys. J. R. Astron. Soc. 47, 41–58.
Markenscoff, X., Dascalu, C., 2012. Asymptotic homogenization analysis for damage amplification due to singular interaction of microcracks. J. Mech. Phys. Solids 60, 1478–1485.
Müller, T.M., Gurevich, B., Lebedev, M., 2010. Seismic wave attenuation and dispersion resulting from wave-induced flow in porous rocks – a review. Geophysics 75 (5). 75A147–75A164.
Nemat-Nasser, S., Deng, H., 1994. Strain-rate effect on brittle failure in compression. Acta Metall. Mater. 42, 1013–1024.
Novikov, S.A., Divnov, I.I., Ivanov, A.G., 1966. Study of rupture of steel, aluminum and copper under explosive loading. Fiz. Met. Metalloved. 21 (4), 23–32.
Paliwal, B., Ramesh, K.T., 2008. An interacting micro-crack damage model for failure of brittle materials under compression. J. Mech. Phys. Solids 56 (3), 896–923.
Papargyri-Beskou, S., Polyzos, D., Beskos, D.E., 2009. Wave dispersion in gradient elastic solids and structures: a unified treatment. Int. J. Solids Struct. 46, 3751–3759.
Peerlings, R.H.J., Fleck, N.A., 2004. Computational evaluation of strain gradient elasticity constants. Int. J. Multiscale Comput. Eng. 2, 599–619.
Ravichandran, G., Subhash, G., 1995. A micromechanical model for high strain rate behavior of ceramics. Int. J. Solids Struct. 32, 2627–2646.
Sanchez-Palencia, E., 1980. Non-homogeneous Media and Vibration Theory. Lecture Notes in Physics, vol. 127. Springer, Berlin.
Smyshlyaev, V.P., Cherednichenko, K.D., 2000. On rigorous derivation of strain gradient effects in the overall behaviour of periodic heterogeneous media. J. Mech. Phys. Solids. 48, 1325–1357.
Taylor, R., 2008. FEAP – A Finite Element Analysis Program – Version 8.2 – User Manual.
Tran, T.-H., Monchiet, V., Bonnet, G., 2012. A micromechanics-based approach for the derivation of constitutive elastic coefficients of strain-gradient media. Int. J. Solids Struct. 49, 783–792.